Materials Research. 2011; 14(1): 113-117
DOI: 10.1590/S1516-14392011005000010

Influence of pH of Colloidal Suspension on the Electrical Conductivity of SnO_2 thin Films Deposited Via Sol-Gel-Dip-Coating

Leandro Piaggi Ravaro*[a], *Luis Vicente de Andrade Scalvi*[b]

[a] *UNESP – State University of São Paulo,*
Postgraduate Program in Materials Science and Technology, Bauru, SP, Brazil
[b] *UNESP – State University of São Paulo, Departament of Physics, Bauru, SP, Brazil*

Received: December 14, 2010; Revised: February 10, 2011

Tin dioxide (SnO_2) thin films are deposited by the dip-coating technique from colloidal suspensions prepared with distinct pH through the sol-gel method. The decrease of the pH contributes to the destruction of an electrical layer adjacent to particles in solution, leading to a high degree of aggregation among these particles due to the generation of cross-linked bonds (Sn-O-Sn) between them. The aggregation affects the electrical properties of films, because the pH variation produces particle with distinct sizes in the film. Undoped samples prepared from pH 6 leads to the highest conductivity among the investigated undoped samples, in agreement with X-ray diffractograms, which indicate higher crystallinity for lower pH. Arrhenius plot evaluated from temperature dependent conductivity data leads to activation energies of the deepest level between 67 to 140 meV, for the films prepared from suspensions with pH 6 to 11. The most probable explanation for this variation in the conductivity and activation energy is related to distinct potential barriers between grains, due to distinct packing caused by cross-linked bonds formed during suspension phase. Characterization of samples lightly doped with Er^{3+} confirms that acid pH leads to higher conductivity, but the highest conduction takes place at even lower pH when compared to undoped thin films.

Keywords: *tin dioxide, sol-gel-dip-coating, electrical conductivity, pH*

1. Introduction

Tin dioxide (SnO_2) thin films are transparent in the visible range and present many types of technological applications such as gas sensors, transparent electrodes, and displays[1-3]. In the undoped form, this semiconductor presents n-type conductivity due to oxygen vacancies and interstitial tin atoms[4], which acts as donors in this matrix. It confers a naturally n-type conduction to this wide bandgap (about 3.6 eV[5,6]) semiconductor. Several techniques have been used for the deposition of tin dioxide thin films: sputtering[7], pyrolysis[8], sol-gel-dip-coating (SGDC)[9]. Each of these techniques provides films with distinct properties. In the SGDC used in this work, the films are obtained from a colloidal suspension and the overall film properties are strongly dependent on the physicochemical characteristics of these suspensions. The variation of pH provided by the experimental procedure influences directly the electrical conductivity of obtained films. The particles in suspension are embedded by an electrical layer[10]. Decreasing the pH may contribute to the destruction of this layer, leading to a high degree of aggregation among particles (clusters) due to the generation of cross-link bonds (Sn-O-Sn)[11] between them (due to the recombination of OH^- groups linked to the particle surface). The aggregation affects the electrical properties of films, due to the higher packing produced by acid pH. Considering the small size of the grains produced by the sol-gel process, the grain boundary scattering must be the dominant mechanism, because the higher packing may lead to larger grains and a lower number of grains throughout the material. Then, the grains surface area is smaller, increasing the grain boundary mobility and then, the electrical conductivity. The pH variation may also contribute for the presence of other compounds, for instance, the synthesis of SnO_2 nanoparticles through the controlled precipitation method leads to distinct compounds depending on the pH[12]. A dominant SnO_2 cassiterite single phase is found in the colloidal suspension at pH values 4.6 and 6.25, however other amorphous complex phases such as chlorides and oxi-chlorides may be present, as revealed by the broadened X-ray difrattogram profile. These phases are dominant when the pH is rather acid. For basic pH 10 the main crystalline phase present is the tin oxy-hydroxide $Sn_6O_4(OH)_4$.

On the other hand, incorporation of Er^{3+} in SnO_2 may contribute for technological innovation, leading to the creation of new opto-electronic devices, such as electroluminescent apparatus[13]. Er^{3+} has high technological potential, due to a large emission range, from the visible to the infrared, specially the emission at about 1540 nm, because it coincides with the minimum absorption of silica-based optical fibers[14,15]. This Er^{3+} infrared emission is indicated for the construction of optical amplifiers to replace electronic converters, decreasing the operation costs[16]. Er^{3+} is incorporated into SnO_2 lattice substitutional in Sn^{4+} sites and exhibits an acceptor-like behavior in tin dioxide, leading to a high degree of electrical charge compensation and high resistivity films. Ion incorporation at grain boundary, caused by low solubility limit of rare-earth ions in SnO_2 (less than 0.1 mol%), may also contribute for low conductivity[17].

In this communication we present electrical characteristics of undoped SnO_2 thin films obtained from colloidal suspensions with distinct pH and the influence of slightly doping with trivalent rare earth ion Er^{3+}. This investigation aims for improvement of gas sensors based on thin films, where the modulated electrical conductivity is the main issue, as well as the knowledge on characteristics of rare-earth trivalent doping.

*e-mail: scalvi@fc.unesp.br

2. Experimental

Colloidal suspensions of SnO_2 undoped and doped with 0.4at% of Er^{3+} have been prepared through the sol-gel route, starting from the preparation of an aqueous solution of $SnCl_4.5H_2O$ (0.5 M). Doping with Er was provided by using the reagent $ErCl_3.6H_2O$. Under stirring with a magnetic bar, NH_4OH was then added until the pH reaches 11, leading to hydrolysis and condensation reactions. The residual precipitate was submitted to dialysis against distilled water for about 10 days, in order to eliminate Cl^- and NH_4^+ ions. This dialysis process was carried out with the help of semi-permeable membranes of Sigma-Aldrich under constant flux of distilled water. This procedure leads to a stable suspension (sol) of undoped SnO_2 or SnO_2:Er with pH 7. For the variation of pH, desired amounts of NH_4OH (basic pH) or HNO_3 (acid pH) were added to the colloidal suspensions, under constant magnetic agitation. The pH was measured and controlled by a pH-meter model DM-10 from Digimed.

Each film layer is deposited at room temperature by the dip-coating technique, followed by gelation in air for 20 minutes and fired at 400 °C for 10 minutes in a furnace at atmospheric pressure. When the total of 10 layers is reached, samples are submitted to thermal annealing at 550 °C for 1 hour in the same furnace. Resulting average thickness of films obtained by this procedure is about 350 nm, as evaluated from scanning electron microscopy of cross section[18,19].

X-ray diffraction data of films were obtained with a RIGAKU diffractometer, model D/MAX-2100/PC, with a scanning rate of 1°/minutes in range of 20-80 degrees.

Tin electrodes deposition onto the SnO_2 thin films were prepared using an EDWARDS auto 500 system, with pressure of about 10^{-5} torr. The substrates were placed close to the Mo crucibles containing small pieces of tin to assure a homogeneous deposition. The whole procedure of placing the metallic electrodes to the SnO_2 film surface is sketched in Figure 1, along with its sequence. All the samples were taken from the same region of the dipped substrate, cutting slices of about 1.0 × 2.6 cm perpendicular to the dipping direction, as shown in Figure 1a. The Sn electrodes are deposited through a shadow mask of Cu as shown in Figure 1b, while the substrate holder rotates, making sure that all the films receive the same amount of evaporated metal. After metal deposition, the samples were annealed at 150 °C for 30 minutes. The evaporation of tin for the electrodes has been used due to the previous best results obtained for SnO_2 films, concerning ohmic behavior and low contact resistance. The schematic representation of the sample cross section is seen in Figure 1c.

Sample cooling for electrical measurements was performed in a He closed-cycle cryostat from APD cryogenics, coupled with a Lake Shore Cryotronics temperature controller with 0.05 degree of precision. The applied bias and the current measurement current were done with the help of a Keithley Electrometer model 6517A.

3. Low Temperature Electrical Characterization of Thin Films

Figure 2 shows resistivity values for films deposited from colloidal suspensions with different pH. The resistivity values are obtained from current-voltage (IxV) measurements carried out at low temperature, along with the sample dimensions as shown in Figure 1. The specific measurement temperatures are: 28, 50, 100 and 150 K. The inset in Figure 2 presents X-ray diffractograms for SnO_2 thin films also obtained from colloidal suspensions with different pH, carried out at room temperature. These diffractograms present the diffuse profile typical of nanocrystallized domain. The labeled peaks correspond to the well-known plans of rutile structure of tin dioxide.

Figure 3 shows current-voltage (I×V) for a typical measurement temperature, 150 K. All the samples present ohmic behavior and very stable signal in the voltage range appointed, leading to precise reproducible data. For the other measurement temperatures (which originated the data of Figure 2), the I×V behavior is quite similar, concerning the linearity of the obtained curves. Only the current magnitude increases with temperature, but the curve shape remains the same. From Figure 3, it is possible to observe that conductivity decreases with decreasing temperature, a typical semiconductor behavior. Besides, there is a conductivity increase with decreasing pH of the colloidal suspension for all the investigated temperatures. For instance, the film obtained from pH 6 presents the lowest resistivity for all the measurement temperatures. It is also useful to mention that the absence of oxygen in the atmosphere where the sample is located has also a strong influence in the sample electrical transport. At 28 K, the pH 6 film presents a resistivity of 17 ohm.cm, whereas

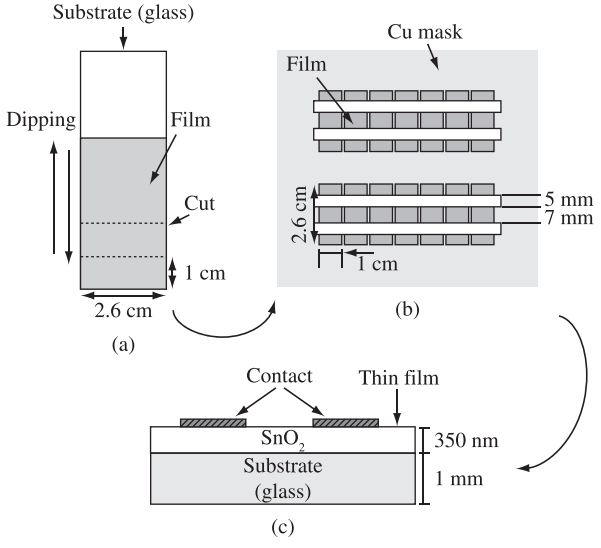

Figure 1. Diagram for the process of obtaining samples for electrical characterization: a) position of the cut slice; b) Cu shadow mask for Sn contact evaporation; c) sample cross section.

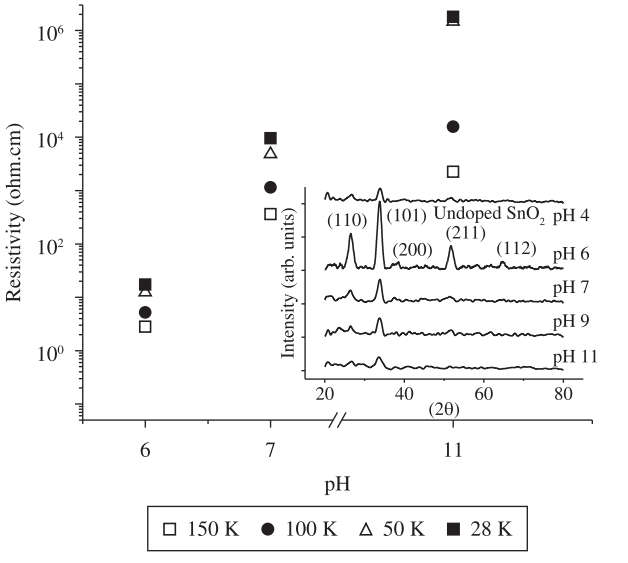

Figure 2. Resistivity of undoped SnO_2 thin films for distinct temperatures and pHs of precursor colloidal suspension. Inset: X-ray Diffratograms for these films.

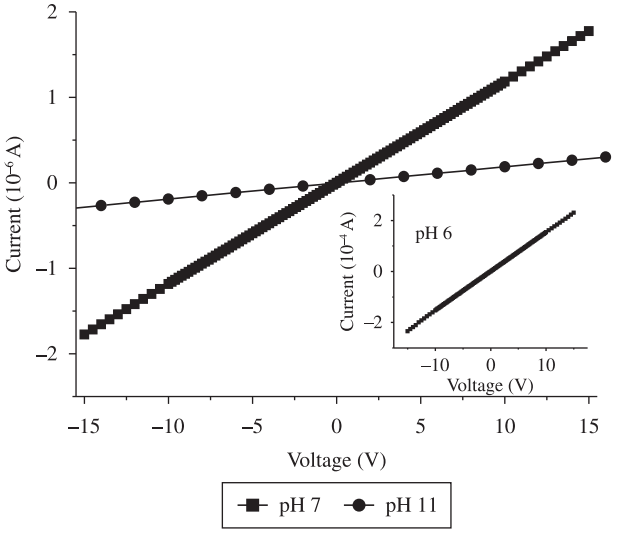

Figure 3. Current-voltage (I×V) for thin films obtained from colloidal suspension with pH 7 and 11, measured at 150K. Inset: I×V for film obtained from pH 6, plotted separately due to much higher magnitude compared to the other samples.

when measured in air, at room temperature, the obtained value was about 110 ohm.cm. The films surface presents adsorbed oxygen species[20,21], which trap electrons from the bulk conduction band, decreasing the conductivity. The adsorbed species can be eliminated by a slight heating process under vacuum conditions. The statistical distribution of charge carriers among the energy levels in the semiconductor generates the effect of trapping electrons back, due to the freezing process. However, considering that measurements at low temperature are carried out in vacuum conditions, the electron trapping is compensated by the electron ionization due to the release of oxygen species from the sample surface.

From the X-ray diffraction data (inset of Figure 2), it is possible to infer that as the pH decreases, the resolution and intensity of the peaks increase until pH 6, decreasing for pH 4. In the X-ray diffraction figure, the main directions of the rutile structure, cassiterite phase are labeled, assuring that, independent on the pH of the colloidal suspension, the obtained thin films still are SnO_2. It seems that there is a limiting value for increasing crystallinity with decreasing pH. Below this value, the cristallinity becomes worse, as can be observed from the inset of Figure 2. It is interesting to notice that the best resolution in the X-ray diffractograms is related to the best electrical conductivity, obtained exactly for films obtained from colloidal suspensions with pH 6. The higher cristallinity obtained for this sample may be related with the sample viscosity, since the lower pH leads to higher viscosity values, resulting in more uniform layers[22] and better defined X-ray diffractograms. On the other hand, the formation of cross-linked bonds between particles[11] during the sol phase may be contributing to the formation of larger colloidal particles, leading to larger crystallites and better definition of the X-ray diffractograms, concomitant with better electrical conductivity for the pH 6 film.

This observation is also helped by the evaluation of the crystallite size through the Scherrer equation[23,24], which is shown in Table 1. The crystallite size is estimated for the (101) direction, which is the most intense for all the diffractograms. It is easily verified that the pH 6 film presents the largest crystallite among all the investigated undoped samples, as expected. Results of atomic force microscopy[25] for undoped SnO_2 shows metallurgical grains of about 30-50 nm, whereas for Er- doped sample the granular surface structure is

Table 1. Evaluation of average crystallite size (t) for SnO_2 thin films in the (101) direction.

pH	t (nm)
4	5.77
6	8.30
7	6.97
9	5.40
11	3.88

destroyed. In doped samples the crystallite are indeed the lowest structure, what does not happen for undoped films. Comparing this grain dimensions with the crystallites estimation shown in Table 1, it may be verified that crystallites become part of a larger domain, composed of metallurgical grains. Independent on the least unit of the material, the better crystallinity and larger particle size obtained for pH 6 assures that the there is a smaller number of particles throughout this sample, leading to better electrical transport due to the decrease of scattering centers.

Figure 4 shows temperature dependent conductivity data for thin films obtained from colloidal suspensions with different pH. The inset in Figure 4 shows the Arrhenius plot calculated from this conductivity data. As the pH of the starting suspension increases from 6 to 11, the electrical conductivity of the films decreases. For films deposited from suspensions with pH 9 and 11, the difference is rather low and, below about 100 K, the conductivity curves crosses each other, resulting that films prepared with pH 9 presents values slightly lower than the ones obtained for pH 11. The proximity of these two curves indicates that the influence of pH of the suspension in the conductivity could be reaching a superior limiting value of the pH influence on the electrical properties. The shape of the conductivity curve for the whole range of investigated temperature and for all the pH, leads to a behavior characteristic of multi-level ionized defects[26,27]. Moreover, it must be taken into account the temperature dependence of mobility. Independent on considering the evaluated crystallite sizes or the metallurgical grains as the scattering unit, the grain boundary scattering is the dominant mechanism and the depletion layer may become as large as half of the crystallite[28]. The mobility due to grain boundary scattering has the general form:

$$\mu_{GB} = CT^{-y} \exp\left(-\frac{qV_{PB}}{kT}\right) \quad (1)$$

Where C is a constant which depends on the grain size and the electron effective mass, and V_{PB} is the potential barrier at grain boundary. The value of the exponent y depends on the equilibrium statistics from where it is derived, varying from 1/2[29] to 1[30]. Then the mobility increases with decreasing temperature, which assures that the conductivity decrease with sample cooling down is indeed due to electron trapping at defects. These multi-level defects are of hard identification due to the continuous variation of the curve slope in the Arrhenius plot. However, it allows evaluating the activation energy for the deepest energy level, ionized at highest measured temperature range. The activation energy calculated from the Arrhenius plot for these films corresponds to the ionization of deep energy levels, and the values are: 67, 89, 135 and 140 meV for pH 6, 7, 9 e 11, respectively. The last two values are in good agreement with the value obtained for the second ionization level of oxygen vacancies[31]. The variation in the deep level activation energy with decreasing pH is a good indication that the random distribution in the local neighborhood, which is being modified as the pH varies, influences the defect level,

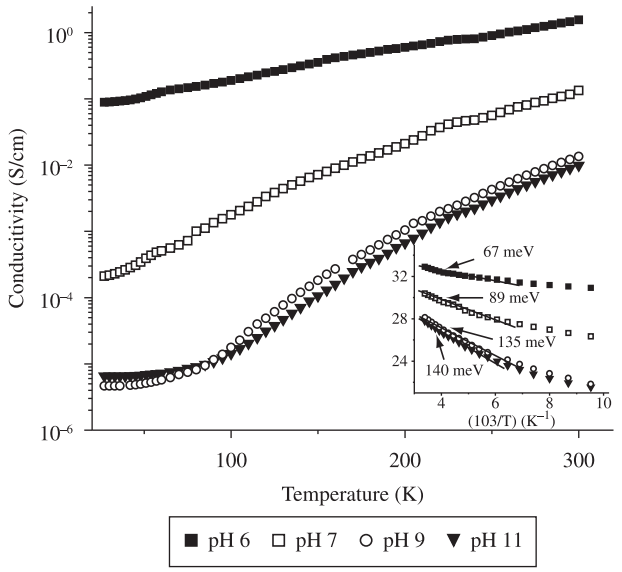

Figure 4. Conductivity as function of temperature for films obtained from pH varying from 6 to 11. Inset: Curves used for the evaluation of activation energy (Ea) for these films. Shown activation energy values are in the range 225 to 300 K.

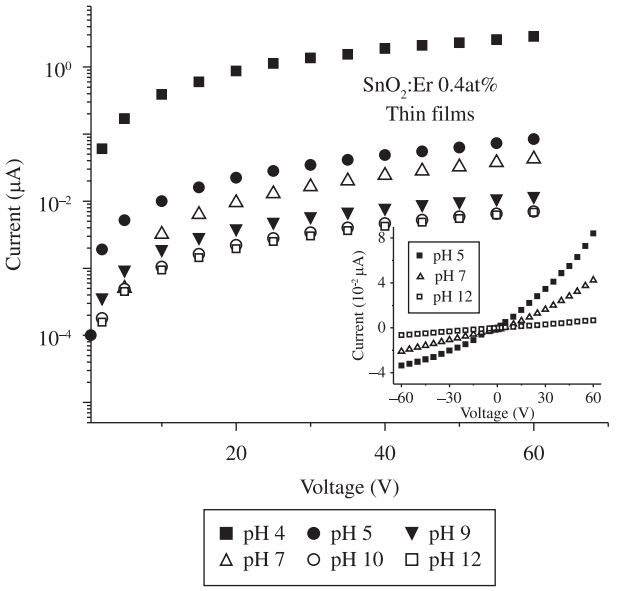

Figure 5. Positive bias of current-voltage data for SnO_2:0.4at%Er^{3+}, obtained from colloidal suspensions with distinct pH, measured at room temperature and pressure conditions, plotted in log scale. Inset: Current-voltage data for selected films obtained from distinct pH, plotted in linear scale.

which becomes closer to the conduction band as the pH decreases. Then, at lower pH, the defect level is being more easily ionized, leading to a higher conductivity as the pH decreases. This result is also in good agreement with the higher crystallinity observed for lower pH. The influence of pH may be related to the adsorption of oxygen species and cross-linked Sn-O-Sn bonds, which is favored for acid pH, changing the potential barrier (V_{PB}) at grain boundary, and then, contributing for higher electronic mobility. The acid pH also influences the expected effect of increasing particles size, which decreases the overall number of particles and then, contributes for the increase of the mobility as well. This influence is very important for the design of gas sensors[32,33], where the basis of application is the modulation of electrical conductivity by adsorbed gaseous species.

Another important feature of the pH variation is the possibility of the presence of other compounds[12] related from the chloride nature of the precursor used to obtain the colloidal suspension. However, no other compound was detected in the X-ray diffractograms as shown in Figure 2. Then, these compounds must be present in small amounts, and the contribution for the electrical conductivity shall not be substantial. However, these characteristics may not be ignored because the best conductivity in this work is coincident with the pH wich favors the single cassiteriste phase in the synthesis of SnO_2 nanoparticles[12].

Figure 5 shows the positive bias part of the I×V behavior of SnO_2 thin films doped with 0.4at% of Er^{3+} obtained from colloidal suspensions with distinct pH. The y-axis is plotted in log scale in order to show the data for all the samples, since the pH 4 has a surprisingly high current compared to the other films. The inset in Figure 5 shows some complete curves for significant pH values, plotted in linear scale. Although the presence of Er^{3+} does not lead to an evident rectification, it leads to some surprising asymmetry. Considering the back-to-back disposition of the contacts (Figure 1), it is expected a rather symmetric I×V behavior. The lack of rectification may be associated with the low Er^{3+} doping concentration, but the observed asymmetry is a feature probably related to non-homogeneities on Er^{3+} distribution on the surface. As already mentioned the Er^{3+} ion has acceptor like behavior in this matrix and a charge compensation process takes place because SnO_2 is naturally n-type. Then, a very high resistivity is expected for Er^{3+}-doped SnO_2 films. Besides, these data were collected under atmospheric pressure condition, which increases the electron trapping by surface adsorbed species. Then, the result shown in Figure 5 for the pH 4 film suggests that the limiting pH value for improving electrical properties depends also on the doping nature. The Er^{3+} doping is located mainly at particles surface due to the low solubility[34]. Then, during the formation of cross-linked bond Sn-O-Sn, the Er^{3+} may influence the process, leading to shorter potential barriers. This result is very interesting for the design of electroluminescent devices, where the electrical conductivity of the SnO_2 sample is the most relevant parameter. This effect is the opposite of the expected variation in conductivity caused by the grain shrinkage due to the presence of doping[17]. Besides, the increase of electrical conductivity for low pH must be taken into account on the design of optoelectronic devices, because the highest infrared emission (about 1540 nm) takes place for pH about 7[35]. Then, a higher conductivity for acid pH must be balanced by a neutral pH for higher emission, in the performance optimization of these devices.

4. Conclusion

Electrical characterization of thin films obtained from colloidal suspension with distinct pH, show that the decrease of pH leads to increasing electrical conductivity. For undoped samples, it seems that there is a limiting pH value for that, which is about pH 6. For lightly Er-doped samples, a lower pH value, 4, leads to even higher conductivity.

Undoped thin films deposited from pH 6 present the highest conductivity, in good agreement with X-ray diffraction data, because the pH 6 sample presented the most intense cassiterite phase peaks and the largest crystallites. The influence of pH may be related to the adsorption of oxygen species and cross-linked Sn-O-Sn bonds during particle formation, which is favored for acid pH, allowing the growth of larger particles and changing the potential barrier at grain boundary, along with the decrease of the number of particles

throughout the sample. The overall effect is increasing the electronic mobility. The Arrehnius plot show that a basic pH leads to activation energy for the deepest level coincident with an oxygen vacancy level, whereas acid pH leads to much lower activation energy, in good agreement with the better conductivity. For Er-doped films, the higher conductivity obtained for pH 4 is probably related to the influence of the particles surface-located rare-earth ions for the formation of the cross linked bonds Sn-O-Sn, decreasing the magnitude of the grain boundary potential barrier.

The investigation of physicochemical properties of the colloidal suspension and the relationship with film properties may lead to the preparation of better quality films and may contribute for the development of new SnO_2-based devices, such as electroluminescent tools. Besides, it may improve the performance of existing devices such as gas sensors, where the main parameter is the material electrical conductivity.

Acknowledgements

Authors would like to thank Brazilian financial sources: CAPES, CNPq and FAPESP.

References

1. Ansari SG, Ansari A, Wahab R, Kim Y, Khang G and Shin H. Glucose sensor based on nano-baskets of tin oxide templated in porous alumina by plasma enhanced CVD. *Biosensors and Bioelectronics*. 2008; 23:1838-1842.
2. Korotkov RY, Farran AJE, Culp T, Russo D and Roger C. Transport properties of undoped and NH_3-doped polycrystalline SnO_2 with low background electron concentrations. *Journal of Applied Physics*. 2004; 96:6445-6453.
3. Giraldi TR, Lanfredi AJC, Leite ER, Escote MT, Varela JA, Longo E et al. Electrical characterization of SnO_2 :Sb ultrathin films obtained by controlled thickness deposition. *Journal of Applied Physics*. 2007; 102:034312-5.
4. Ray SC, Karanjai MK and Dasgupta D. Tin dioxide based transparent semiconducting films deposited by the dip-coating technique. *Surface and Coatings Technology.*1998; 102(1-2):73-80.
5. Mulvaney P, Grieser F and Meisel D. Electron transfer in aqueous colloidal tin dioxide solutions. *Langmuir.* 1990; 6(3):567-572.
6. Tagliente MA, Bello V, Pellegrini G, Mattei G, Mazzoldi P, Massaro M et al. Synthesis and characterization of SnO_2 nanoparticles embedded in silica by ion implantation. *Nuclear Instruments and Methods in Physics Research B*. 2010; 268:3063-3065.
7. Gorley PM, Khomyak VV, Bilichuk SV, Orletsky IG, Horley PP and Grechko VO. SnO_2 films: formation, electrical and optical properties. *Materials Science and Engineering: B*. 2005; 118:160-163.
8. Paraguay-Delgado F, Miki-Yoshida M, Antunez, W, Gonzales-Hernandez J, Vorobiev YV and Prokhorov E. Corrigendum to "Morphology and microstructure of textured SnO_2 thin films obtained by spray pyrolysis and their effect on electrical and optical properties. *Thin Solid Films.* 2008; 516:4293-4294.
9. Shuping G, Jing X, Jianqiao L and Dongxiang Z. Highly sensitive SnO_2 thin film with low operating temperature prepared by sol-gel technique. *Sensors and Actuators B: Chemical*. 2008; 134:57-61.
10. Gouvea D and Murad BBS. Influence of acid-basic characteristic of Al_2O_3 or SnO_2 surfaces on the stability of ceramic suspensions with commercial dispersants. *Cerâmica.* 2001; 47:51-56.
11. Hiratsuka RS, Santilli CV, Silva DV and Pulcinelli SH. Effect of Electrolyte on the Gelation and Aggregation of SnO_2 Colloidal Suspensions. *Journal of Non-Crystalline Solids.* 1992; 147-8:67-73.
12. Ararat Ibarguen C, Mosquera A, Parra R, Castro MS and Rodriguez-Paez, JE. Synthesis of SnO_2 nanoparticles through the controlled precipitation route. *Materials Chemistry and Physics.* 2007; 101:433-440.
13. Perea-Lopez N, Gonzalez-Ortega JÁ and Hirata, GA. Electroluminescence from Eu^{3+} doped Sr_2CeO_4 nanocrystalline thin films. *Optical Materials*. 2006; 29:43-46.
14. Coffa S, Franzò, G, Priolo F, Polman A and Serna R. Temperature dependence and quenching processes of the intra-4f luminescence of Er in crystalline Si. *Physical Review B*. 1994; 49:16313-16320.
15. Castañeda-Contreras J, Meneses-Nava MA, Barbosa-García O, Rodríguez-Rojas RA and Félix MV. Visible erbium luminescence in SiO_2:TiO_2:Er^{3+} sol-gel powders. *Optical Materials*. 2006; 29:38-42.
16. Kenyon AJ. Recent developments in rare-earth doped materials for optoelectronics. *Progress in Quantum Electronics*. 2002; 26:225-284.
17. Morais EA and Scalvi LVA. Electron trapping of laser-induced carriers in Er-doped SnO_2 thin films. *Journal of the European Ceramic Society*. 2007; 27:3803-3806.
18. Geraldo V, Scalvi LVA, Morais EA, Santilli CV and Pulcinelli SH. Sb Doping Effects and Oxygen Adsorption in SnO_2 Thin Films Deposited via Sol-Gel. *Materials Research*. 2003; 6(4):451-456.
19. Pineiz TF, Scalvi LVA, Saeki MJ and Morais EA. Interface Formation and Electrical Transport in SnO_2:Eu^{3+}/GaAs Heterojunction Deposited by Sol–Gel Dip-Coating and Resistive Evaporation. *Journal of Electronic Materials.* 2010; 39(8):1170-1176.
20. Yamazoe N, Fuchigami J, Kishikawa M and Seiyama T. Interactions of tin oxide surface with O_2, H_2O and H_2. *Surface Science.* 1979; 86:355-344.
21. Belmonte JC, Manzano J, Arbiol J, Cirera A, Puigcorbé J, Vila A et al. Micromachined twin gas sensor for CO and O_2 quantification based on catalytically modified nano-SnO_2. *Sensors and Actuators B*. 2006; 114:881-892.
22. Carvalho DM, Maciel Jr JLB, Ravaro LP, Garcia RE, Ferreira VG and Scalvi LVA. Numerical simulation of the liquid phase in SnO_2 thin film deposition by sol-gel-dip-coating. *Journal of Sol-Gel Science and Technology.* 2010; 55:385-393.
23. Cullity BD and Stock R. *Elements of X-ray diffraction*. 3rd. ed. New Jersey: Prentice Hall, 2001.
24. Bose AC, Thangadurai P and Ramasamy S. Grain size dependent electrical studies on nanocrystalline SnO_2. *Materials Chemistry and Physics.* 2006; 95:72-78.
25. Morais, EA, Scalvi LVA, Ravaro LP, Siu Li M and Floriano EA. Optical and Transport Properties of Rare-earth Trivalent Ions Located at Different Sites in Sol-gel SnO_2. *Journal of Physics: Conference Series.* 2010; 249:012005.
26. Blakemore JS. *Semiconductor statistics*. New York: Dover publications; 1987.
27. Jarzebski ZM, Marton JP. Physical Properties of SnO_2 Materials, I. Preparation and Defect Structure. *Journal of The Electrochemical Society.*1976; 123:199C-205C.
28. Watson J, Ihokura K and Coles, GSV. The tin dioxide sensor. *Measurement Science and Technology.* 1993; 4:711-719.
29. Zhang DH and Ma HL. Scattering Mechanisms of charge carriers in transparent conducting oxide films. *Applied Physics A*. 1996; 62:487-492.
30. Bruneaux J, Cachet H, Froment M, Messad A. Correlation between Structural and Electrical properties of Sprayed Tin Oxide films with and without Fluorine doping. *Thin Solid Films.* 1991; 197:129-142.
31. Samson S, Fonstad CG. Defect structure and electronic donor levels in stannic oxide crystal. *Journal of Applied Physics*. 1973; 44:4618-4621.
32. Guglielmi M, Menegazzo E, Paolizzi M, Gasparro G, Ganz D, Putz J et al. Sol-Gel Deposited Sb-Doped Tin Oxide Films. *Journal of Sol-Gel Science and Technology.* 1988; 13:679-683.
33. Adamovicz B, Izydorczyk W, Izydorczyk J, Klimasek A, Jakubik W and Zywicky J. Response to oxygen and chemical properties of SnO_2 thin-film gas sensors. *Vacuum*. 2008; 82:966-970.
34. Morais EA, Ribeiro SJL, Scalvi LVA, Santilli CV, Ruggiero LO and Pulcinelli SH. Optical characteristics of Er^{3+}–Yb^{3+} doped SnO_2 xerogels. *Journal of Alloys and Compounds*, 2002; 344:217-220.
35. Ravaro LP, Tabata A, Oliveira JBB and Scalvi LVA. Raman and photoluminescence of Er^{3+}-doped SnO_2 obtained via the sol–gel technique from solutions with distinct pH. *Optical Materials.* 2010; 33:66-70.